RESEARCH PAPER

Heat Treatment Effects on Microstructure, Hardness & Corrosion of Al-12Si-Cu Alloy

Asaad Kadhim Eqal[1,*], Haider Akram Hussein[2]

* *asaad.kadhim@stu.edu.iq*

[1] Department of Mechanical Techniques, Amarah Technical Institute, Southern Technical University, Basrsh 62001, Iraq
[2] Department of Applied Mechanics, Engineering Technical College-Baghdad, Middle Technical University, Baghdad 10074, Iraq

Received: November 2025 **Revised: February 2026** **Accepted: August 2026**
DOI: 10.22068/ijmse.4421

Abstract: *This work systematically explores the influence of different heat-treatment parameters, namely solutionizing and artificial ageing conditions, on the microstructure, mechanical hardness, and corrosion resistance of Al-12Si-Cu alloy. Solution treatment was performed at two temperatures (500°C and 530°C) and two durations (0.5 and 3 hours), and artificial aging was performed at two temperatures (180°C and 310°C) over two durations (2 and 5 hours). Optical microscopy also showed microstructural changes, including fine grain refinement, enhanced spheroidization of the coarse eutectic Si phase, and a more uniform distribution of primary intermetallic grains. These structural adjustments were identified as direct determinants of properties of the material. Maximum microhardness (155 HV) was achieved at 500°C/3 h solutionizing and 180°C for 5 h ageing (S3), which was ascribed to successful solid-solution strengthening and fine precipitation hardening. In contrast, the lowest hardness (54 HV) was obtained at 530°C/3 h + 310°C/5 h (S8), showing the harmful impact of over-ageing at higher temperatures. Electrochemical corrosion analysis detected a significant correlation between corrosion resistance and the treated microstructure, where conditions favouring microstructural refinement resulted in a decrease in corrosion current density. A Design of Experiments (DOE) method using the Taguchi L8 orthogonal array was used to determine how each parameter contributed relative to the other variables. The analysis revealed that, while ageing temperature was the most influential factor on microhardness, solution time was the controlling factor for surface roughness. The results demonstrate a robust determination of the main processing windows, which are crucial for enhancing particular properties, and confirm the strong feasibility of temperature control in heat-treatment process optimisation to balance mechanical strength and corrosion performance in Al-12Si-Cu alloys.*

Keywords: *Al-Si-Cu alloy, Heat treatment, Aging, Corrosion, Optimization.*

1. INTRODUCTION

Aluminum–silicon-based alloy systems, specially the Al-12Si aluminum alloy system, are utilized to play vital roles in the automobile, aerospace and offshore industries. They are increasingly used because of their good castability, low density, high specific strength, and inherent corrosion performance [1–3]. The important enhancement of the mechanical and thermal performance of the alloy by supplementary alloying elements like copper Cu and magnesium Mg can be achieved efficiently. More precisely, this is facilitated by effective precipitation hardening and significant microstructural improvement [4, 5]. In all Al-Si systems, the Al-12Si-Cu system has drawn growing attention from practitioners for its high strength-to-weight ratio, low fabrication cost, and good ability to form complex casting geometries [6]. At this stage, copper can be readily introduced by direct application and forms the intermetallic phase Al2Cu. This is important for strengthening the alloy by fine-tuning solution or ageing treatments [7, 8]. The resultant microstructure, particularly the shapes, sizes, and spatial areas of silicon particles, eutectic phases and strengthening precipitates, play an essential role in determining the final mechanical performance of Al-Si-Cu alloys [9, 10]. Solution treatment, typically carried out at high temperatures, allows all secondary phases to dissolve completely. Automated ageing then causes the gradual precipitation of strengthening phases (e.g., metastable θ' (Al_2Cu)) required for significant hardness and yield strength [11]. In recent years, scientists have relied heavily on statistical design tools (e.g., RSM and the Taguchi method) to systematically optimise complex heat treatment parameters (solution temperature, ageing temperature, and holding time). For instance, Pezda et al. [12] investigated the impact of T6 heat treatment parameters on the EN AC-AlSi12CuNiMg aluminum alloy modified with strontium and cast into metal molds. The optimal solutioning was achieved at 535°C for 3 hours, followed by immediate quenching in water at 20°C. This stage ensured maximum dissolution of copper-rich and magnesium-rich phases into the aluminum matrix. Similarly, Raju, K., et al. [13] highlighted that the heat treatment (solutionizing at 510°C, ageing at 220°C) of Al-15Si-6Ni-2Cu alloy induced Si particle spheroidization and precipitation of Ni-rich and Al_2Cu phases. The 4 h aged alloy achieved optimal performance, reducing the wear rate by up to 45% with significantly lower friction compared to the as-cast state, whereas over-ageing caused precipitate coarsening and degraded wear behavior. Studies by dos Santos et al. [14] and Wiengmoon et al. [15] show that heat treatment can facilitate or degrade corrosion resistance markedly based on the continuity, stability, and electrochemical potential of the precipitated intermetallics, which typically serve as active cathodic sites. Moreover, thermal cycling may unintentionally lead to surface roughness and modification of the surface energy profile, with resultant effects on mechanical properties and the system's local susceptibility to corrosion mechanisms [16]. Therefore, efficient tuning of these coupling parameters is essential for optimising final alloy performance under severe industrial conditions. Despite extensive research, a notable gap remains: a significant lack of multi-response experimental work examining the combined effects of solution and ageing treatment on Al-12Si-Cu alloys, with simultaneous microhardness and surface roughness, as well as corrosion resistance, comparisons. In contrast, previous work has mostly focused on mechanical and electrochemical characteristics individually [17–18]. In an attempt to fill this gap, this study strives to systematically evaluate the impact of four parameters: solution temperature 500°C, 530°C, solution time 0.5 h, 3 h, aging temperature 180°C, 310°C, aging time 2 h, 5 h on the microstructure, microhardness, surface roughness, and corrosion behavior of Al-12Si-Cu alloys by adopting the Taguchi L8 orthogonal array design.

2. EXPERIMENTAL PROCEDURES

2.1. Theory and Formula

This work employs Taguchi experimental design. The Taguchi method uses an orthogonal array (OA), a fractional factorial design, to identify the best combination with fewer experiments and less time [19]. Table 1 illustrates the factors and levels for the process. It considers solution temperature (500-530°C), solution time (0.5-3 hr), aging temperature (180-310°C), and aging time (2-5 hr). Although, the Taguchi approach requires only 8 experiments to obtain the optimal levels (Table 3) of variables, while to optimize on all factors at two levels, the best solution approach needs 16 tests (2^4= 16), which are practically exhausting. Thus, the Taguchi approach can rapidly identify crucial components, reducing time, cost, and the number of tests [20]. The artificial-ageing levels were set at 180°C and 310°C. While 180°C represents the conventional peak-aging temperature for Al-Si-Cu alloys, the higher temperature of 310°C was strategically selected to investigate the material's behavior under extreme over-aging conditions, which is critical for evaluating the thermal stability of engine components operating at elevated temperatures [21].

As indicated in Table 2, the experiments were carried out using the standard L8 orthogonal matrix based on the Taguchi method, using the statistical program MINITAB 21. The Taguchi method evaluates the quality characteristics using the signal-to-noise (S/N) ratio, where a higher S/N ratio indicates a more robust design. Depending on the type of quality response, three criteria are commonly applied: "larger-is-better", "nominal-is-better", and "smaller-is-better". Each criterion has its own advantages, and the corresponding S/N ratio is calculated according to the following formula [22]:

$$\begin{cases} \left(S/N_1 = 10\log\left(\frac{1}{n}\sum_{i=1}^{n} y_i^2\right)\right) \\ \left(S/N_2 = 10\log\left(\bar{y}^2/\widehat{\sigma^2}\right)\right) \\ \left(S/N_3 = -10\log\left(\frac{1}{n}\sum_{i=1}^{n} y_i^2\right)\right) \end{cases} \quad (2.1)$$

In this study, the experimental data were transformed into signal-to-noise (S/N) ratios. The "larger-is-better" criterion was applied for hardness, while the "smaller-is-better" criterion was adopted for surface roughness.

Table 1. Factors and levels for the process

Factor	Symbol	Unit	Level	
			Level 1	Level 2
Solution temperature	A	°C	500	530
Solution time	B	hr	0.5	3
Aging temperature	C	°C	180	310
Aging time	D	hr	2	5

[DOI: 10.22068/ijmse.4421]

Table 2. L8 design matrix with corresponding experimental results

Exp. No.	Coded parameters				Un-Coded parameters			
	A	B	C	D	Solution temperature	Solution time	Aging temperature	Aging time
1	1	1	1	1	500	0.5	180	2
2	1	1	2	2	500	0.5	310	5
3	1	2	1	1	500	3.0	180	2
4	1	2	2	2	500	3.0	310	5
5	2	1	1	1	530	0.5	180	2
6	2	1	2	2	530	0.5	310	5
7	2	2	1	1	530	3.0	180	2
8	2	2	2	2	530	3.0	310	5

2.2. Materials

In this work, an Al–Si–Cu alloy was chosen as the reference (base) material. Table 3 presents the alloy's chemical composition. Cylindrical specimens with a diameter of 1.5 cm were cut and processed. The specimens' surfaces were prepared using a metallographic process (i.e., sequential grinding with silicon carbide (SiC) abrasive papers of different grit sizes, followed by polishing with a cloth impregnated with alpha-alumina suspension) to obtain a smooth, reflective surface for micro-structure and surface testing.

2.3. Heat Treatment

The heat-treatment process was designed based on known principles of solid-solution strengthening and precipitation kinetics for Al-Si-Cu alloys. It is done in two steps: solution treatment followed by artificial aging. First, the samples were solution treated at 500°C and 530°C for 0.5 and 3 hours, respectively, followed by immediate cold-water quenching. This temperature scale was chosen for processing at a temperature just below the theoretical eutectic melting point (close to 577°C) for the Al-Si framework, to maximise the dissolution of critical hardening phases of the Al matrix (e.g., Al_2Cu and Si), without burning phase locally (local melting) in the alloy structure [23]. The kinetic restriction on phase dissolution was evaluated by varying the time. Second, the artificial ageing was carried out at two temperature ranges (180°C and 310°C) for 2 and 5 hours. These temperatures were chosen to represent the two major regimes of precipitation behaviour: 180°C is the standard peak-age hardening temperature, where fine, metastable precipitates form maximally to achieve maximum strength. 310°C was used to study precipitation phases under severe overaging, characterised by precipitate coarsening and non-strengthening phases. This allows a better inspection of the transition from maximum strength to structural stability and deterioration. All heat-treatment procedures were performed in a Carbolite 1200-type furnace in the Metallurgical Laboratory at the Department of Materials Engineering, University of Technology–Baghdad. The varying heat-treatment schedules were coded as S0–S8 for clarity, and the specific conditions are summarised in Table 4.

Table 3. Chemical composition of Al-Si-Cu alloy

Element	Si	Cu	Mg	Fe	Zn	Ni	Mn	Ti	Cr	Al
Wt%	12.587	3.563	1.168	0.857	0.683	0.513	0.335	0.070	0.049	Bal.

Table 4. Conditions of heat treatments

Specimen Label	Solution Temp (°C)	Solution Time (hr)	Aging Temp (°C)	Aging Time (hr)
S0	Untreated sample			
S1	500	0.5	180	2
S2	500	0.5	310	5
S3	500	3.0	180	5
S4	500	3.0	310	2
S5	530	0.5	180	5
S6	530	0.5	310	2
S7	530	3.0	180	2
S8	530	3.0	310	5

[DOI: 10.22068/ijmse.4421]

2.4. Microhardness and Roughness

Microhardness testing of untreated and heat-treated samples was conducted with an HVS-1000 micro-hardness tester (manufactured by LARYEE) using the micro-indentation protocol as recommended by ASTM E384 and ISO 6507 [24]. The indenter was a Vickers diamond indenter, and the load applied was 9.8 N for 15 s under constant load [25]. Hardness was measured at several locations for each sample, and the average value was recorded. Surface roughness measurements were carried out using a TA 620 measuring platform with a handheld roughness gauge (TR200) and a portable roughness gauge (TR240) to capture surface texture accurately. Potentiodynamic polarization tests were performed using a WINKING MLab 200 Potentiostat (Bank-Elektronik, Germany) with a standard three-electrode electrochemical cell. The electrochemical measurements were performed with SCI electrochemical analysis software at a scan rate of 3 mV/s, with the polarisation scans performed after the open-circuit potential Eocp was stabilised. The stabilization criterion was defined in terms of less than 5 mV variation over 10 minutes (as a steady state before polarization) that is congruent with most electrochemical tests. The key electrochemical characteristics obtained were the corrosion potential (Ecorr) and corrosion current density (icorr), determined by Tafel extrapolation. The Tafel slopes were also calculated, to further elucidate the anodic and cathodic behavior of the alloy surfaces, across heat treatment conditions.

3. RESULTS AND DISCUSSION

3.1. Microstructures

The as-cast microstructure of Al–Si alloys is composed primarily of large primary α-Al grains, acicular eutectic silicon, and coarse primary silicon particles. Moreover, adverse intermetallic phases such as needle-like β-Al_5FeSi severely affect the alloy's mechanical properties [5, 26]. The aluminum in the eutectic phase of unmodified Al–Si alloys displays crystalline features comparable to those of the primary α-Al dendrites [6]. The typical microstructure of the hypoeutectic Al–Si alloy is composed of α-Al grains and dendrites surrounded by eutectic silicon, which is found as elongated acicular structures or as fine rounded particles. The shape of the acicular Si can be changed to a more fibrous shape using suitable chemical modifiers. An optical microstructure of the Al–Si alloy employed in this work is shown in Fig. 1a and shows the presence of primary α-Al, acicular eutectic Al–Si, and coarse silicon particles [27]. Copper in Al-Si alloys forms intermetallic compounds, including Al_2Cu, during solidification. This phase may form block-like particles or lamellar structures that alternate with the α-Al matrix. The Al_2Cu precipitates are often concentrated in the interdendritic area, thereby enhancing mechanical strength. Further, iron could form additional intermetallics like Cu_2FeAl_7 or $Al_5Cu_2Mg_8Si_6$ depending on the specific solidification conditions. The microstructural properties of the Al-12Si-Cu alloy were affected by different solution and aging treatments. The untreated sample (S0) had coarse primary α-Al dendrites and long acicular eutectic silicon, as well as intermetallic phases such as blocky Al_2Cu and needle-like β-Al_5FeSi, but the treatment produced significant microstructural refinement. Figs (1 a to i) demonstrate the fragmentation, but also partial morphological transformation, of eutectic Si induced by short treatments (e.g., S1 and S2). In comparison, specimens after prolonged solution time and during high-temperature ageing (e.g., S5–S8) showed more homogeneous structures, with significant spheroidization of eutectic Si and dissolution of coarse intermetallics. This two-stage transformation fragmentation followed by spheroidization was especially evident in S8 (530°C/3 h + 310°C/5 h), where the microstructure was completely homogenized with fine, rounded silicon particles dispersed in the α-Al matrix. These findings emphasise that heat-treatment parameters play an essential role in facilitating eutectic Si granulation and refining overall alloy structure, further strengthening mechanical and corrosion performance [28]. Additional analysis of the heat-treatment response for the Al-Si-Cu alloy shows that treatment at a solution temperature of 500°C decreases the average size of silicon particles, eventually causing fragmented segments to become more spheroidal. In contrast, treatment at 530°C for 0.5 hours causes silicon particles to neck and separate into segments that hold their original shape. This partially realised transformation may result in coarsening of eutectic silicon. After treatment with solutions at 530°C for 3 hours and then aging of the alloy, heterogeneous nucleation is significantly increased–a dominant factor in grain refinement. The microstructural analysis reveals a significant morphological transformation of the eutectic Si phase. In the as-cast condition, Si particles appear as coarse acicular plates with a high aspect ratio (typically >5). Following the optimised solution treatment at 500°C, these particles fragment and spheroidize, substantially reducing the aspect ratio toward a more spherical geometry (approaching 1.5–2.0). Such a process results in nucleation of foreign phases only in specific locations, which grow slowly in the molten matrix. Also, when copper, magnesium, and iron are present, many intermetallic species are produced, including Al_2Cu, Mg_2Si, α-$Al_{12}(Fe, Mn)_3Si_2$, and β-Al_5FeSi. Together with the formation of a fine, fibrous eutectic silicon structure during solidification, these compounds significantly affect the alloy's mechanical and corrosion performance. An Al-Si-Cu alloy precipitation sequence relies on the formation of crystalline Al_2Cu-based precipitates. The Al_2Cu precipitation sequence is described as follows in [9-11]:

$$\alpha ss \rightarrow \text{GP Zones} \rightarrow \theta'' \rightarrow \theta' \rightarrow \theta \text{ (Al2Cu} \quad (3.1)$$

3.2. Microhardness and Roughness

Each of the applied heat treatment and aging steps mentioned in Fig. (2) significantly affected the microhardness and surface roughness of the Al-12Si-Cu alloy.

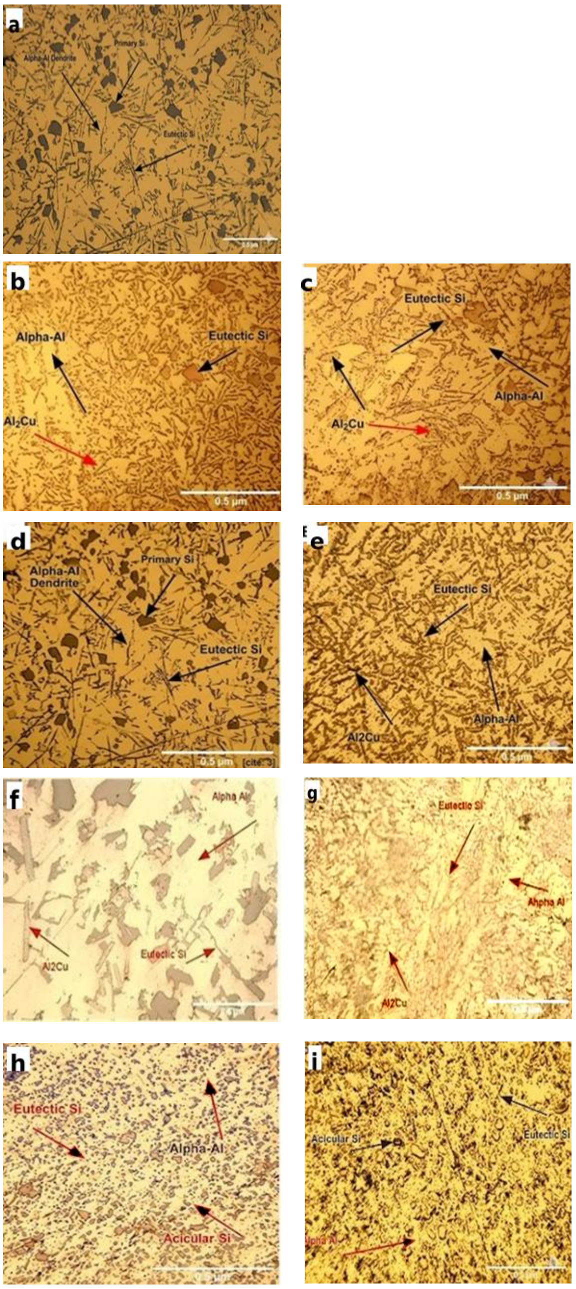

Base metal of Al-Si alloy before heat treatment

Microstructures after heat treatment at 500°C and 0.5 hrs followed by b) aging at 180°C for 2 hrs, c) aging at 310°C for 5 hrs

Microstructures after heat treatment at 500°C and 3 hrs followed by d) aging at 180°C for 5 hrs, and e) aging at 310°C for 2 hrs

Microstructures after heat treatment at 530°C and 0.5 hrs followed by: f) aging at 180°C for 5 hrs, and g) aging at 310°C for 2 hrs

Microstructures after heat treatment at 530°C and 3 hrs followed by: (h) aging at 180°C for 2 hrs. (i) aging at 310°C for 5 hrs

Fig. 1. Microstructures after and before heat treatment

[DOI: 10.22068/ijmse.4421]

Heat treatment and ageing significantly affected the microhardness of the modified Al-Si-Cu alloy. At a fixed solution temperature and holding time, it was observed that lower aging temperatures yielded higher microhardness values. This is probably because the coherent precipitates that form during ageing inhibit dislocation motion and contribute to alloy strengthening. By appropriately tuning the ageing parameters (temperature and time), an extensive range of mechanical properties can be obtained [30]. After solution treatment and quenching, the matrix is supersaturated with solute atoms and vacancies. This supersaturation allows rapid atomic clustering, resulting in Guinier-Preston (GP) zones. These zones then become metastable coherent or semi-coherent precipitates, either directly or through the dissolution of GP zones, and thus contribute to strengthening [31].

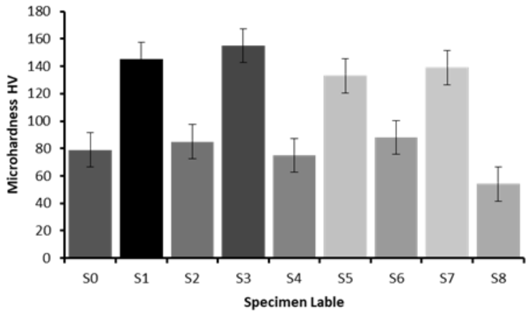

Fig. 2. Variation of microhardness with specimen labels

The highest microhardness value (155 HV) was recorded for specimen S3, which was solution-treated at 500°C for 3 hours and aged at 180°C for 5 hours among the tested samples. These results corroborate those of [32]. In contrast, specimen S8 (treated at 530°C for 3 hours and aged at 310°C for 5 hours) showed low microhardness, which may be associated with over-ageing and precipitate coarsening. S3 was investigated by optical microscopy, where good grain refinement, especially in the small sections, is observed, which results in high hardness as shown in Fig. 3. Moreover, a small increase in surface roughness was observed following heat treatment and aging, which is ascribed to many fine precipitates and small size refinement of the structural phases [33]. The significant decrease in microhardness observed at 310°C can be attributed to the accelerated precipitation kinetics. According to the precipitation sequence in Al-Si-Cu alloys ($\alpha ss \rightarrow$ GP Zones $\rightarrow \theta'' \rightarrow \theta' \rightarrow \theta$) aging at 310°C promotes the rapid coarsening of the semi-coherent θ′ phase and its subsequent transformation into the coarse, incoherent stable θ (Al2Cu) phase. This transformation leads to a loss of coherency with the aluminum matrix, thereby reducing the pinning effect on dislocation movement [34].

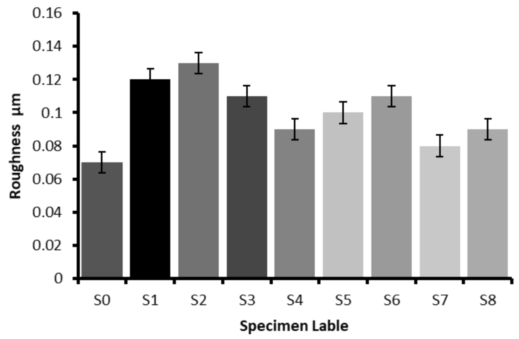

Fig. 3. Variation of Roughness with specimen labels

3.3. Corrosion Behavior

The potentiodynamic polarization curves for unmodified versus heat-treated Al-Si alloys are depicted in Figs (4) and (5). These curves have two specific reactions in the active region. The lower curve is the cathodic reaction, namely the reduction of the dissolved oxygen, denoted by this reaction:

$O_2 + 2H_2O + 2e \rightarrow 4OH^-$ (4.1).

In contrast, the upper part of the polarisation curve denotes the anodic reaction, where oxidation of the aluminium alloy takes place. Typically, this reaction is described as follows:

$Al \rightarrow Al^{3+} + 3e$ (4.2).

Changes in the anodic and cathodic branches of treated and untreated samples may demonstrate the effects of heat treatment on corrosion behaviour, passive film stability, and electrochemical properties of the precipitated intermetallic phases. Table (5) summarises the potentiodynamic polarisation results and shows that corrosion behaviour in these specimens varies significantly. The untreated sample, S0, showed a corrosion potential (Ecorr) of (–611 mV) and a corrosion rate (CR) of 32.48 mpy, providing a reference for performance comparison. The thermal regime was applied to each studied class, and significant variations followed the heat treatment. Among the specimens treated at 500°C, S1 (0.5 h + aging at 180°C for 2 h) showed a significant change in corrosion performance, Ecorr= –679 mV and CR= 4.76 mpy, indicating good corrosion resistance and improved microhardness (145 HV) compared to S0. Conversely, S3 (500°C at 3 h plus aging at 180°C at 5 h) had the greatest hardness (155 HV) and moderate roughness (0.11 µm), and the highest corrosion (35.07 mpy) rate, indicating

[DOI: 10.22068/ijmse.4421]

effective mechanical strength-corrosion compromise. Specimen S4 showed the worst corrosion performance, despite treatment at 500°C for 3 h and ageing at 310°C for 2 h, with a corrosion rate of 142.89 mpy, likely due to coarsened intermetallics acting as galvanic couples. At 530°C, S5 (0.5 h + aging at 180°C for 5 h) and S7 (3 h + aging with 180°C for 2 h) had a better balance between the two values, in particular, for S7, the most noble Ecorr= –436 mV with CR= 17.32 mpy, indicating better passivation but a moderate corrosion rate. S8 had the weakest hardness (54 HV), and achieved negligible corrosion resistance (CR= 31.63 mpy), suggesting it was suboptimal. Taking into account the three main parameters, hardness, roughness, and rate of corrosion, S1 has the best combination and provides good corrosion resistance, adequate hardness, and moderate surface roughness. Overall, there was a modest influence of heat treatment on the corrosion behavior and considerable differences can be explained by the appearance or dissolution of specific microstructural features. For 500°C, short solution treatment (0.5 h) with aging facilitated a decrease in corrosion rates, possibly caused by the formation of Guinier–Preston (GP) zones and coherent/semi-coherent precipitates to reduce microgalvanic coupling. However, with long-term treatment (3 h), the zones might dissolve, and the susceptibility to corrosion would increase. In contrast, at 530°C the solution time increased to 3 h, which led to a lower corrosion rate due to improved intermetallic refinement and eutectic Si fragmentation, as indicated by optical and roughness data. This delicate microstructure also resulted in fewer localised anodic/cathodic sites and attenuated corrosion evolution [12, 13, 35].

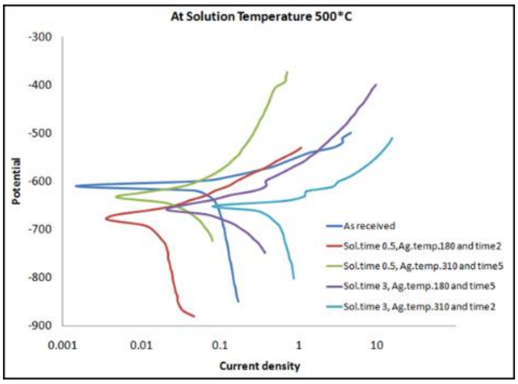

Fig. 4. Tafel polarization plots of as-received and heat-treated specimens at 500°C solution temperature with varying solution times (h), aging temperatures (°C), and aging times (h)

Moreover, the high surface roughness reported among specimens (e.g., S2) may also relate to enhanced susceptibility to corrosion as rough surfaces offer more active sites for electrolyte penetration and localized corrosion. As a result, the hardness, roughness, and microstructural refinement are balanced to improve corrosion resistance. Specimen S2 displayed the greatest surface roughness (0.13 μm), which may relate to the formation of coarse intermetallic phases from ageing at 310°C for 5 h. S8 showed only moderate roughness (0.09 μm) despite having the lowest hardness (54 HV), supporting the possibility that the thermal conditions resulted in spheroidization and therefore did not prevent precipitation hardening. The potentiodynamic polarisation results (Table 5) indicate that corrosion performance varied among the observed samples. For example, sample S0 showed a corrosion potential (Ecorr) of -611 mV and a corrosion rate (CR) of 32.48 mpy, respectively, and was used as an intermediate sample to compare corrosion behaviour. When heat was applied, prominent changes were observed depending on the application temperature. For 500°C-treated samples, S1 (0.5 h) + aging at 180°C for (2 h) resulted in remarkable improvement, as evidenced by Ecorr= –679 mV and CR= 4.76 mpy, with good corrosion resistance and superior micro-hardness (145 HV) to S0. Notably, an optimal balance between mechanical performance and corrosion protection was achieved. Accordingly, S3 (500°C for 3 h + aging at 180°C for (5 h)) showed the highest hardness (155 HV) but a much higher corrosion rate (35.07 mpy). This indicates that the thermal conditions that favour optimal precipitation strength may also facilitate the formation of closer and more continuous networks of micro-galvanic sites. In contrast, the worst corrosion performance (CR= 142.89 mpy) occurred in S4, which was treated for (3 h) at 500°C but aged for (2 h) at 310°C, probably because coarsened intermetallics are highly efficient galvanic couples. S7 (3 h + aging at 180°C) at 530°C for (2 h) had the most noble Ecorr= –436 mV and a moderate corrosion rate (17.32 mpy) indicating better passivation. Following the trend, S8 also exhibited the lowest hardness (54 HV) and no visible corrosion improvement (CR 31.63 mpy), confirming its suboptimal performance—mechanics: Microstructure and corrosion. Corrosion resistance is determined by the morphological variation resulting from the heat treatment. The effect of heat treatment on

[DOI: 10.22068/ijmse.4421]

corrosion behaviour is moderate but complex. At 500°C, shorter solution treatment (0.5h) and aging (S1) contribute to reduced corrosion rates, which might be attributed to the formation of fine Guinier–Preston (GP) regions and coherent precipitates. By consuming local Cu atoms contained in the matrix, these fine precipitates form a solute-depleted region adjacent to the particles. This region effectively diminishes the differential driving micro-galvanic coupling in the system. However, long-term treatment (3 h) may cause these areas to dissolve or coarsen, increasing vulnerability. By contrast, conditions that induced reduced corrosion rates, especially those with a higher 530°C solution temperature and longer times (e.g., S7), showed improved intermetallic refinement and eutectic Si fragmentation.

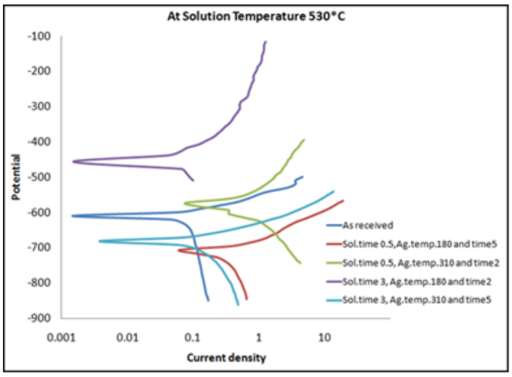

Fig. 5. Tafel polarization plots of as-received and heat-treated specimens at 530°C solution temperature with varying solution times (h), aging temperatures (°C), and aging times (h)

This change is supported by the optical and roughness data, which show a more streamlined microstructure that plays a major role in corrosion. Si spheroidization (the process requested by the reviewer) plays an important role here, in that it breaks the continuous linear path of the Si eutectic network to form a lot more small (isolated) particles of the large, continuous cathodic network. This morphological change efficiently lowers the active surface area of the cathodic phase. It shrinks the length scale over which galvanic cells can function, resulting in fewer localised anodic/cathodic sites and reduced corrosion propagation. Moreover, some specimens (e.g., S2, 0.13 μm) exhibit greater surface roughness, which can also indicate increased susceptibility to corrosion; a rougher surface provides more active sites for electrolyte penetration and localised corrosion. Thus, ultimate corrosion resistance results from the interplay between precipitation hardening, which may enhance galvanic coupling, and microstructural refinement and Si spheroidization, which physically impede cathodic routes.

3.4. Optimization and Statistical Analysis (Taguchi Method)

3.4.1. Probability plots

A probability plot is an easy way to determine whether a data set satisfies a hypothesised distribution. The data are plotted against an ideal distribution, and if the plot is a straight line, it can reasonably be assumed that the observed statistical sample is from the ideal distribution. Deviations from that line indicate departures from the distribution. To test the normality assumption of the experimental data, the Anderson-Darling test (ADT) is applied. The ADT is an efficient statistical tool to detect deviations from normality and is particularly useful for studying outliers [36]. Fig. 6 shows that these data are nearly linear, and the p-value is greater than 0.05. This indicates that the experimental data follow a normal distribution, supporting further study and refinement.

3.4.2. Mean effects plot for means

The main effect plots of the composite are depicted in Fig. (7), and the main effect plot for mean hardness, as shown in Fig. (7-a), indicates that hardness decreases with an increase in solution temperature, solution time, aging temperature, and aging time (500-530°C, 0.5-3 hr, 180-310°C, 2-5 hr).

Table 5. Properties of Al-Si alloy before and after heat treatments

Specimen Label	Microhardness (HV)	Roughness (μm)	Ecorr (mV)	icorr (μA/cm^2)	CR(mpy)
S0	79	0.07	-611	75	32.48
S1	145	0.12	-679	11	4.76
S2	85	0.13	-634	24	10.39
S3	155	0.11	-657	81	35.07
S4	75	0.09	-651	330	142.89
S5	133	0.10	-706	190	82.27
S6	88	0.11	-574	312	135.10
S7	139	0.08	-436	40	17.32
S8	54	0.09	-681	73	31.63

[DOI: 10.22068/ijmse.4421]

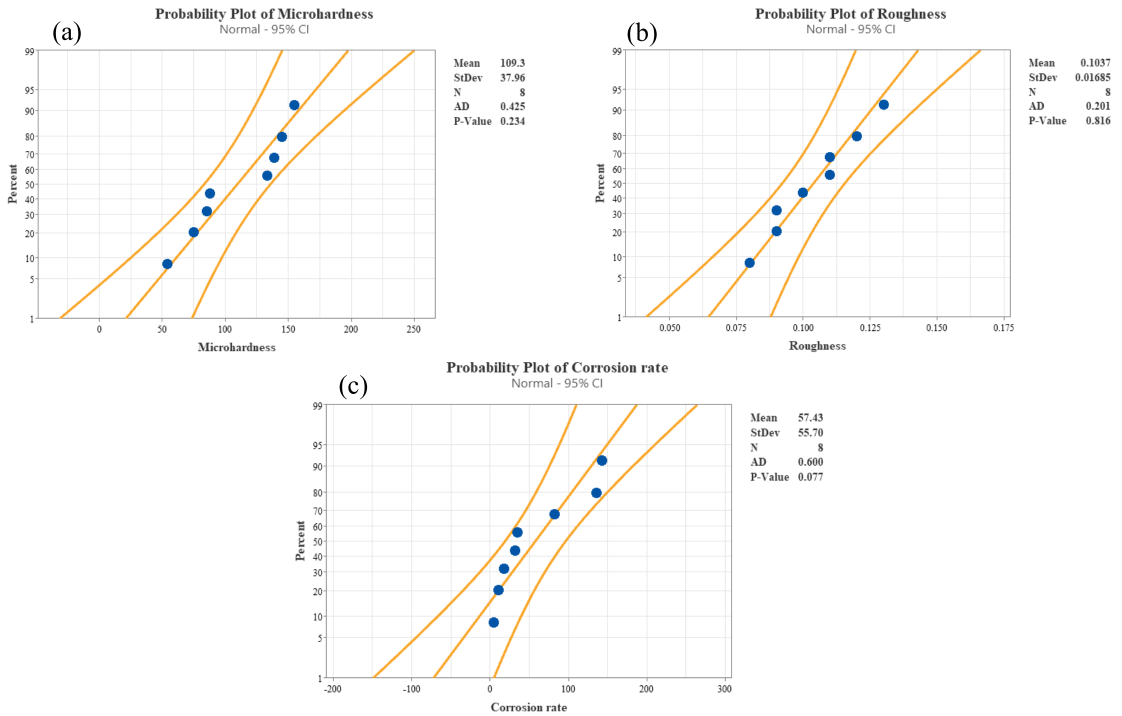

Fig. 6. Probability Plot of a) Microhardness, b) Roughness, c) Corrosion rate

For mean roughness, Fig.(7-b) shows the main effect plot, which indicates that roughness increases with an increase in solution temperature, aging temperature, and aging time (500-530°C, 180-310°C, 2-5 hr) and decreases linearly with an increase in solution time (0.5-3). Finally, see the main effect plot for mean corrosion rate from Fig. (7-c), depicting how corrosion rate increases with an increase in solution temperature and aging temperature (500-530°C, 180-310°C). Also, the corrosion rate decreases linearly with increasing solution time and ageing time (0.5-3, 2-5) hr.

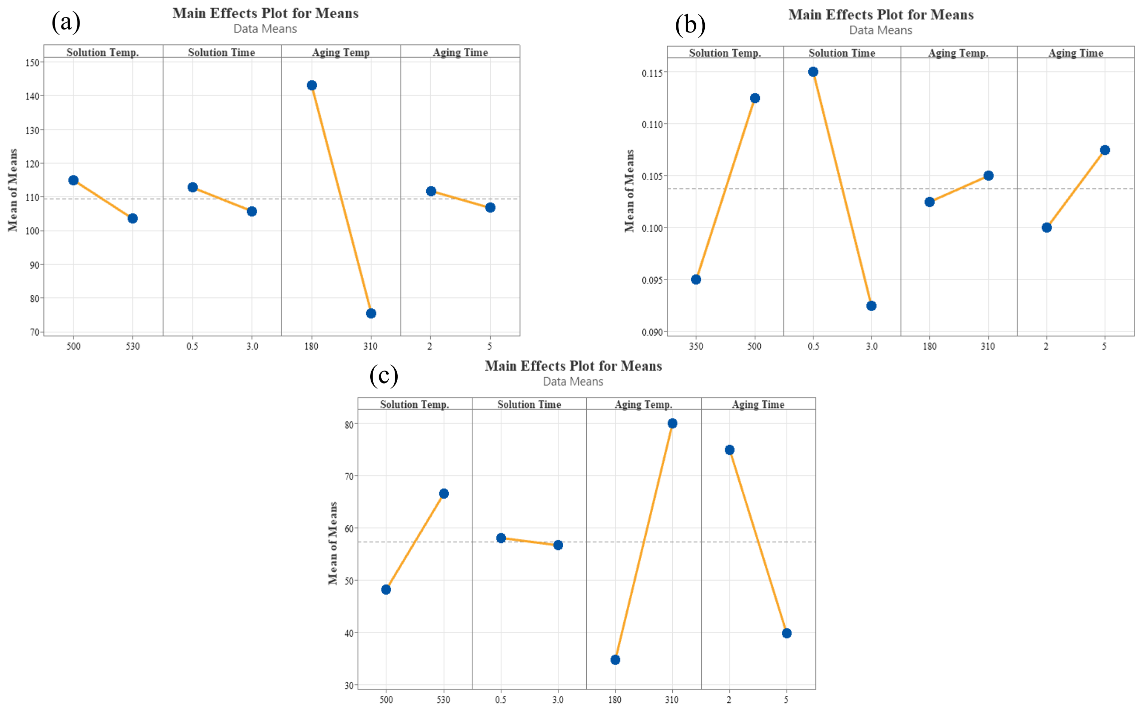

Fig. 7. Mean effect plot for the mean of a) Microhardness, b) Roughness, c) Corrosion rate

[DOI: 10.22068/ijmse.4421]

3.4.3. *Single objective optimization*

Individual responses are optimized in terms of signal to noise (S/N) ratios [37]. In this study, we have several functions for individual responses, namely maximizing hardness and minimizing both corrosion rate and roughness. Therefore, Equation (1) is used to apply the "larger is better" property for hardness, and Equation (2) is used for corrosion rate and roughness. Table 6 shows the signal-to-noise ratio for each factor using the Minitab 21 analytical program. Regarding the signal-to-noise ratio (SNR) for the hardness test, as shown in Table 6, the highest SNR was 43.8066 for Experiment 3, which had (solution temperature, aging temperature, and aging time at Level 1, respectively, and solution time at Level 2). For roughness, the highest SNR was for Experiment 7 (21.9382), which had (solution temperature, solution time, and aging time at Level 2, and aging temperature at Level 1). Finally, for corrosion rate, the highest SNR was -13.5521 for Experiment 1, which had (solution temperature, solution time, aging temperature, and aging time at Level 1, respectively). The optimum levels were obtained from the average signal-to-noise ratios, as shown in Fig. (8). For hardness, all factors were optimal at Level 1. For roughness, three factors (solution temperature, aging temperature, and aging time) were optimal at Level 1, while solution time was optimal at Level 2. For corrosion rate, three factors (solution temperature, solution time, and aging temperature) were optimal at Level 1, whereas aging time was optimal at Level 2.

Table 6. Results: Signal-to-noise ratio using for each test L8 OA

Experimental number	Signal to noise ratio		
	Hardness test	Roughness	Corrosion rate
1	43.2274	18.4164	-13.5521
2	38.5884	17.7211	-20.3323
3	43.8066	19.1721	-30.8987
4	37.5012	20.9151	-43.1000
5	42.4770	20.0000	-38.3048
6	38.8897	19.1721	-42.6131
7	42.8603	21.9382	-24.7710
8	34.6479	20.9151	-30.0020

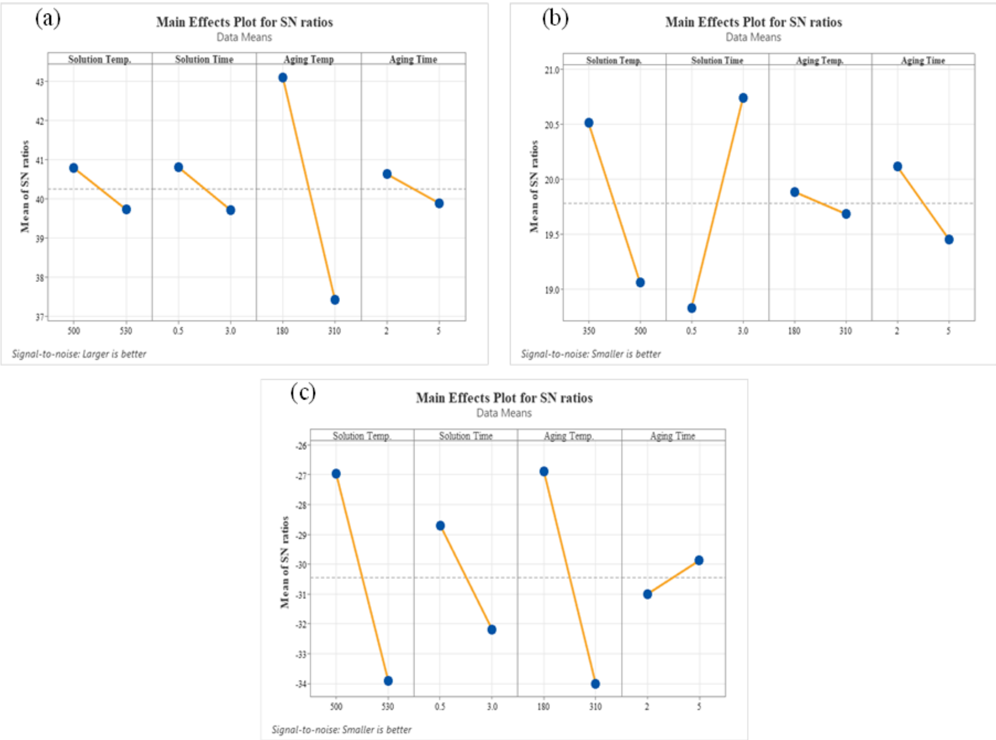

Fig. 8. Main effects plots for the signal-to-noise (S/N) ratios of a) Microhardness, b) Surface roughness, and c) Corrosion rate

[DOI: 10.22068/ijmse.4421]

3.4.4. *Analysis of variance*

The main purpose of the Analysis of Variance (ANOVA) was to obtain an estimate of the magnitude and impact of each heat treatment parameter on the final material properties. Analysis was performed within a 95% confidence interval. Normally, a $P< 0.05$ is needed to show statistical significance of a factor. The ANOVA results (Table 7) presented showed that P-values for most of the 3 factors (microhardness of the material, surface roughness of the material and corrosion rate) were greater than 0.05. This result—common to Taguchi L8 orthogonal array designs, which make minimal use of degrees of freedom for error estimation—implies that, although the factors are not universally statistically significant at the 95% confidence level in this particular experimental model, the analysis will be key for unveiling the prevailing trends and the relative hierarchy of factor influence [38].

The percentage contribution does not show statistical significance, but provides significant information about the underlying physics of the process:

- Microhardness: The aging temperature (84.152%) was the most contributing factor, which goes hand-in-hand with precipitation kinetics as the strongest mechanism for strength enhancement. Next were solution time (3.101%), solution temperature (2.936%) and aging time (1.423%).
- Surface roughness: The solution time (51.548%) dominated the outcome, and solution temperature (29.786%) was the second main contributor, indicating that final surface quality is largely dependent upon the dissolution and micro-structural homogenization.
- Corrosion rate: Aging temperature (12.8671%) and solution temperature (12.231%) played an almost equal role and demonstrated complex interaction of precipitation morphology and phase dissolution on electrochemical behavior.

The error contribution in the ANOVA analysis (approximately [X]%) is attributed to uncontrollable factors such as minor fluctuations in furnace temperature and the inherent variability in the manual polishing process during microstructure preparation. Since the Taguchi L8 design focuses on main effects, the interaction terms were pooled into the error term, confirming that the individual parameters, especially aging temperature, are the primary drivers of the alloy's performance. The best results suggest a compromise between mechanical and corrosion properties. For S1, the lowest corrosion rate (4.76 mpy) was attained, and the highest hardness (155 HV) was attained at S3. Multi-objective optimisation (Taguchi S/N and ANOVA analyses for all responses) can identify different processing windows to maximise each property, guiding future engineering activities. Therefore, the ideal responses are adapted to suit the end-use-the S3 design is optimal for strength applications and S1 for corrosion requirements. The enhancement in corrosion resistance (4.76 mpy) is attributed to two synergistic effects. First, the spheroidization of eutectic Si particles reduces the number of sharp edges, which typically act as localized cathodic sites for pit initiation.

Table 7. ANOVA results

Test	Source	DF	Seq SS	Adj SS	Adj MS	F	P	%Concentration
Hardness test	Solution Temp.	1	2.256	2.256	2.256	1.05	0.381	2.936
	Solution Time	1	2.383	2.383	2.383	1.11	0.369	3.101
	Aging Temp	1	64.662	64.662	64.662	30.11	0.012	84.152
	Aging Time	1	1.094	1.094	1.094	0.51	0.527	1.423
	Residual Error	3	6.443	6.443	2.148			8.385
	Total	7	76.839					
Roughness test	Solution Temp.	1	4.2060	4.20600	4.20600	7.47	0.072	29.786
	Solution Time	1	7.2790	7.27900	7.27900	12.94	0.037	51.548
	Aging Temp.	1	0.0806	0.08063	0.08063	0.14	0.730	0.57
	Aging Time	1	0.8669	0.86688	0.86688	1.54	0.303	6.139
	Residual Error	3	1.6882	1.68821	0.56274			11.955
	Total	7	14.1207					
Corrosion rate	Solution Temp.	1	96.658	96.658	96.658	0.51	0.525	12.231
	Solution Time	1	24.393	24.393	24.393	0.13	0.743	3.0868
	Aging Temp.	1	101.679	101.679	101.679	0.54	0.516	12.8671
	Aging Time	1	2.529	2.529	2.529	0.01	0.915	0.3200
	Residual Error	3	564.962	564.962	188.321			71.494
	Total	7	790.222					

Second, the optimized heat treatment leads to a more uniform distribution of Cu-rich intermetallics, minimizing the formation of severe galvanic couples between the α-Al matrix and the precipitates. According to the ANOVA results, aging temperature was the most influential factor, as it controls the degree of Cu-precipitation and the subsequent electrochemical stability of the alloy surface.

4. CONCLUSIONS

According to a combined study of the heat treatment, microstructure, hardness, surface roughness, and corrosion characteristics of Al-12Si-Cu alloy, the following conclusions are deduced:

1. Microstructural control: Heat treatment and aging are the most applicable to engineered microstructure. The procedure also promoted intense segmentation and spheroidization of the eutectic silicon (Si) phase and converted coarse primary intermetallic particles into a more refined, uniformly distributed morphology.
2. Mechanical Properties: The alloy mechanical properties are highly dependent on controllable precipitation kinetics. The highest microhardness (155 HV) occurred in the S3 condition (500°C 3 h + 180°C 5 h), optimal for maximum precipitation hardening. The lowest hardness (54 HV) also indicates that prolonged ageing at high aging temperature (530°C 3 h + 310°C 5 h) results in severe overage and related loss of strength.
3. The corrosion behaviour is microstructurally state-dependent and characterised by its mechanisms and performance. For specimen S1 (500°C 0.5 h + 180°C 2 h), the most satisfactory corrosion resistance (lowest corrosion rate of 4.76 mpy) was recorded. This improvement can mainly be traced to enhanced microstructure and spheroidization of the eutectic Si network, which effectively alters the continuous cathodic path and reduces micro-galvanic coupling, thus inhibiting corrosion growth.
4. Trade-Off and Factor Effects: The results show a clear trade-off between the conditions that enhance hardness (e.g., S3) and those which reduce corrosion resistance; and vice versa. Based on Taguchi analysis, ageing temperature was identified as the most important parameter controlling mechanical and corrosion properties, with solution time considered more proportional to factor performance, indicating the importance of thermal kinetics.
5. Optimization Results: The particular processing windows for each optimal target property are adequately defined in this work. The optimal conditions for maximum strength (S3) and best corrosion protection (S1) are well characterised and will offer useful recommendations for industrial applications of Al-12Si-Cu alloys.

ACKNOWLEDGEMENTS

The authors thank Southern Technical University and Middle Technical University for providing the laboratory facilities and technical support needed to conduct the experimental part of this research.

REFERENCES

[1] Dash, S. S. and Chen, D., "A Review on Processing–Microstructure–Property Relationships of Al–Si Alloys: Recent Advances in Deformation Behavior". Metals, 2023, 13, 609.

[2] Eshaghi, A., Ghasemi, H. M. and Rassiza Dehghani, J., "Effect of Heat Treatment on Microstructure and Wear Behavior of Al–Si Alloys with Various Iron Contents". Mater. Des., 2011, 32, 1520–1525.

[3] Nnakwo, K. C., Nwajioke, C. T., Chukwuneke, J. L., Ugwuanyi, B. C., Ogbunaoffor, K. C. and Ozoh, C. C., "Microstructure Evolution in A356 Alloy Subjected to Controlled Heat Treatment Regimes Processes". Discov. Appl. Sci., 2024, 6, 497.

[4] Callegari, B., Lima, T. N. and Coelho, R. S., "The Influence of Alloying Elements on the Microstructure and Properties of Al–Si-Based Casting Alloys: A Review". Metals, 2023, 13, 1174.

[5] Mohamed, A. M. A. and Samuel, F. H., "Heat Treatment of Al–Si–Cu/Mg Casting Alloys". In: Heat Treatment: Conventional and Novel Applications, 2012, 55.

[6] Zhang, N "Microstructure Evolution and Mechanical Properties of Al–12Si–xCu–yNi–1Mg Alloy with Different Ni/Cu Ratios". Mater. Today Commun., 2024, 38, 108081.

[7] Abdelaziz, M. H., Elgallad, E. M., Doty, H. W. and Samuel, F. H., "Strengthening Precipitates and Mechanical Performance

[DOI: 10.22068/ijmse.4421]

of Al–Si–Cu–Mg Cast Alloys Containing Transition Elements". Mater. Sci. Eng. A, 2021, 820, 141497.
[8] Zhang, M., Tian, Y., Zheng, X., Zhang, Y., Chen, L. and Wang, J., "Research Progress on Multi-Component Alloying and Heat Treatment of High Strength and Toughness Al–Si–Cu–Mg Cast Aluminum Alloys". Materials, 2022, 12, 1065.
[9] Xie, Y., Liu, S., Guo, X. and Deng, Y., "Development of Ultra-High Strength Al–Cu–Li Alloys Containing High Mg through the Combination of Pre-Stretching and Age-Hardening". Mater. Sci. Eng. A, 2024, 896, 146289.
[10] Sinnwell, Y., Maksakov, A., Palis, S. and Antonyuk, S., "Influence of the Particle Morphology on the Spray Characteristics in Low-Pressure Cold Gas Process". Powder Technol., 2025, 464, 121084.
[11] Bahl, S., Xiong, L., Allard, L. F., Michi, R. A., Poplawsky, J. D., Chuang, A. C., Singh, D., Watkins, T. R., Shin, D., Haynes, J. A. and Shyam, A., "Aging Behavior and Strengthening Mechanisms of Coarsening Resistant Metastable θ′ Precipitates in an Al–Cu Alloy". Mater. Des., 2021, 198, 109378.
[12] Pezda, J., "The Effect of the T6 Heat Treatment on Hardness and Microstructure of the EN AC-AlSi12CuNiMg Alloy". Metalurgija, 2014, 53, 63–66.
[13] Raju, K., Jagadeesha, T., Alavandi, M. R., Kurahatti, R. V. and Goudar, D. M., "Effect of Aging Time on the Microstructure and the Wear Behavior of Al–15Si–6Ni–2Cu Alloy". J. Mater. Eng. Perform., 2026.
[14] Dos Santos, S. L., Tolockzo, F. R., Merij Neto, A. C., Cezario, F. E. M., da Silva, D. M. and Antunes, R. A., "Microstructural Evolution and Corrosion Behavior of Non-Isothermally Heat Treated Hypoeutectic Al–Si–Cu Alloy". Next Mater., 2024, 5, 100262.
[15] Wiengmoon, A., Sukchot, P., Tareelap, N., Pearce, J. T. H. and Chairuangsri, T., "Effects of T6 Heat Treatment with Double Solution Treatment on Microstructure, Hardness and Corrosion Resistance of Cast Al–Si–Cu Alloy". Arch. Metall. Mater., 2015, 60, 881–886.
[16] Xie, D., Wang, Z., Zhou, X., Cheng, X. and Li, X., "Effect of Different Laser Energy Densities on the Corrosion Resistance of Aluminum Alloys". Anti-Corros. Methods Mater., 2020, 67, 437–444.
[17] Korkmaz, A., Yağcı, T. and Çulha, O., "A Computational and Experimental Approach to the Enhancement of Heat Treatment Processes for Al–Si–Mg Alloys". J. Alloys Compd., 2025, 1035, 181468.
[18] Cabrini, M., Lorenzi, S., Testa, C., Pastore, T., Manfredi, D., Lorusso, M., Calignano, F. and Fino, P., "Statistical Approach for Electrochemical Evaluation of the Effect of Heat Treatments on the Corrosion Resistance of AlSi10Mg Alloy by Laser Powder Bed Fusion". Electrochim. Acta, 2019, 305, 459–466.
[19] Bayati, A., Ahmadi, M., Rahmatabadi, D., Khodaei, M., Xiang, H., Baniassadi, M., Abrinia, K., Zolfagharian, A., Bodaghi, M. and Baghani, M., "3D Printed Elastomers with Superior Stretchability and Mechanical Integrity by Parametric Optimization of Extrusion Process Using Taguchi Method". Mater. Res. Express, 2025, 12, 015301.
[20] Shojaei, S., Shojaei, S., Band, S. S., Kazemzadeh Farizhandi, A. A., Ghoroqi, M. and Mosavi, A., "Application of Taguchi Method and Response Surface Methodology into the Removal of Malachite Green and Auramine-O by NaX Nanozeolites". Sci. Rep., 2021, 11, 16054.
[21] Jung, J.-G., Park, J.-S. and Lee, Y.-K., "Quantitative Analyses of Dissolution and Precipitation Kinetics of θ-Al_2Cu Phase in an Al-6.2Si-2.9Cu Alloy Using Electrical Resistivity". Metals Mater. Int., 2013, 19, 147–152.
[22] Wu, H., Li, H., Wang, X., Yang, J., Jiang, R., Deng, X. and Wang, J., "Research on Multi-Objective Optimization Design for High-Precision Turning-Milling Machine Tool Bed Based on Taguchi Method–FEA". Sci. Rep., 2025, 15, 27307.
[23] Jang, J.-H., Nam, D.-G., Park, Y.-H. and Park, I.-M., "Effect of Solution Treatment and Artificial Aging on Microstructure and Mechanical Properties of Al–Cu Alloy". Trans. Nonferrous Met. Soc. China, 2013, 23, 631–635.
[24] International Organization for Standardization, "Metallic Materials—Vickers Hardness Test—

Part 1: Test Method (ISO 6507-1:2018)". ISO, Geneva, 2018.
[25] Eqal, A. K., Yagoob, J. A. and Hussein, H. A., "Investigation of the Effect of TiC on Some Properties of ZA-27 Alloy Prepared by Powder Metallurgy Method". Mater. Res., 2024, 27, e20240143.
[26] Zhao, G., Xing, Z., Li, M., Gao, S., Tao, J. and Chai, S., "Research on Microstructure and Growth Mechanism of Different Primary Silicon in Hypereutectic Aluminum Alloy". J. Phys. Conf. Ser., 2022, 2152, 012022.
[27] Rashed, H. M. M. A., Ashrafi, E. A. and Hasan, A., "Modelling Effects of Copper on Microstructure and Properties of Al–Si–Cu Alloys". Mater. Trans., 2023, 64, 177–183.
[28] Sivarupan, T., Taylor, J. A. and Cáceres, C. H., "Effect of Si and Cu Content on the Size of Intermetallic Phase Particles in Al-Si-Cu-Mg-Fe Alloys". In: Shape Casting: 5th International Symposium, 2014, 161–168.
[29] Ibrahim, A. I., Elgallad, E. M., Samuel, A. M., Doty, H. W. and Samuel, F. H., "Effects of Addition of Transition Metals on Intermetallic Precipitation in Al–2%Cu–1%Si-Based Alloys". Int. J. Metalcast., 2018, 12, 574–588.
[30] Ringer, S. P. and Hono, K., "Microstructural Evolution and Age Hardening in Aluminium Alloys: Atom Probe Field-Ion Microscopy and Transmission Electron Microscopy Studies". Mater. Charact., 2000, 44, 101–131.
[31] Wang, H., Deng, W. and Wang, S., "Precipitates Generation Mechanism and Surface Quality Improvement for Aluminum Alloy 6061 in Diamond Cutting". J. Wuhan Univ. Technol. Mater. Sci. Ed., 2024, 39, 150–159.
[32] Sui, Y., Jiang, Y. and Wang, Q., "Effect of Solution Treatment on Microstructure and Mechanical Properties of As-Cast Al-12Si-4Cu-2Ni-0.8Mg-0.2Gd Alloy". China Foundry, 2022, 19, 238–244.
[33] Amith, V. K., Baloor, S. S., Polishetty, A., Bolar, G. and Govindhan, A. N., "Heat Treatment and Its Effect on Machining Induced Surface Roughness of Cast and Additive Manufactured AlSi10Mg". Sci. Rep., 2025, 15, 26433.
[34] Heugue, P., Larouche, D., Breton, F., Massinon, D., Martinez, R. and Chen, X.-G., "Precipitation Kinetics and Evaluation of the Interfacial Mobility of Precipitates in an AlSi7Cu3.5Mg0.15 Cast Alloy with Zr and V Additions". Metals, 2019, 9, 777.
[35] Rocha, W. F. C., Prado, C. B. and Blonder, N., "Comparison of Chemometric Problems in Food Analysis Using Non-Linear Methods". Molecules, 2020, 25, 3025.
[36] Qazi, M. I., Akhtar, R., Abas, M., Khalid, Q. S., Babar, A. R. and Pruncu, C. I., "An Integrated Approach of GRA Coupled with Principal Component Analysis for Multi-Optimization of Shielded Metal Arc Welding (SMAW) Process". Materials, 2020, 13, 3457.
[37] Lingam, D., Ananthanarayanan, R., Jeevanantham, A. K. and Seenivasagam, D. R., "Optimization Methods in Powder Metallurgy for Enhancing the Mechanical Properties: A Systematic Literature Review". Eng. Res. Express, 2024, 6, 022504.